



Article

The Effect of Ethanol on Disassembly of Amyloid- β_{1-42} Pentamer Revealed by Atomic Force Microscopy and Gel Electrophoresis

Atsuya Matsui ¹, Jean-Pierre Bellier ^{2,*} , Takeshi Kanai ¹, Hiroki Satooka ¹, Akio Nakanishi ¹, Tsukasa Terada ³, Takafumi Ishibe ³, Yoshiaki Nakamura ³, Hiroyasu Taguchi ², Nobuyasu Naruse ^{1,*} and Yutaka Mera ¹

¹ Department of Fundamental Bioscience, Shiga University of Medical Science, Otsu 520-2192, Japan; ds111877@g.shiga-med.ac.jp (A.M.); ds111623@g.shiga-med.ac.jp (T.K.);

hsatooka@belle.shiga-med.ac.jp (H.S.); nakanisi@belle.shiga-med.ac.jp (A.N.); mera@belle.shiga-med.ac.jp (Y.M.)

² Molecular Neuroscience Research Center, Shiga University of Medical Science, Otsu 520-2192, Japan; taguti@belle.shiga-med.ac.jp

³ Graduate School of Engineering Science, Osaka University, 1-3 Machikaneyama-Cho, Toyonaka 560-8531, Japan; u897541f@ecs.osaka-u.ac.jp (T.T.); ishibe.takafumi.es@osaka-u.ac.jp (T.I.); nakamura.yoshiaki.es@osaka-u.ac.jp (Y.N.)

* Correspondence: bellier@belle.shiga-med.ac.jp (J.-P.B.); naruse@belle.shiga-med.ac.jp (N.N.); Tel.: +81-77-548-2101 (N.N.)



Citation: Matsui, A.; Bellier, J.-P.; Kanai, T.; Satooka, H.; Nakanishi, A.; Terada, T.; Ishibe, T.; Nakamura, Y.; Taguchi, H.; Naruse, N.; et al. The Effect of Ethanol on Disassembly of Amyloid- β_{1-42} Pentamer Revealed by Atomic Force Microscopy and Gel Electrophoresis. *Int. J. Mol. Sci.* **2022**, *23*, 889. <https://doi.org/10.3390/ijms23020889>

Academic Editors: Luigi Casella, Paolo de Girolamo and María Trinidad Herrero

Received: 13 December 2021

Accepted: 12 January 2022

Published: 14 January 2022

Publisher's Note: MDPI stays neutral with regard to jurisdictional claims in published maps and institutional affiliations.



Copyright: © 2022 by the authors. Licensee MDPI, Basel, Switzerland. This article is an open access article distributed under the terms and conditions of the Creative Commons Attribution (CC BY) license (<https://creativecommons.org/licenses/by/4.0/>).

Abstract: The most common type of dementia, Alzheimer's disease, is associated with senile plaques formed by the filamentous aggregation of hydrophobic amyloid- β ($A\beta$) in the brains of patients. Small oligomeric assemblies also occur and drugs and chemical compounds that can interact with such assemblies have attracted much attention. However, these compounds need to be solubilized in appropriate solvents, such as ethanol, which may also destabilize their protein structures. As the impact of ethanol on oligomeric $A\beta$ assembly is unknown, we investigated the effect of various concentrations of ethanol (0 to 7.2 M) on $A\beta$ pentameric assemblies ($A\beta_p$) by combining blue native-PAGE (BN-PAGE) and ambient air atomic force microscopy (AFM). This approach was proven to be very convenient and reliable for the quantitative analysis of $A\beta$ assembly. The Gaussian analysis of the height histogram obtained from the AFM images was correlated with band intensity on BN-PAGE for the quantitative estimation of $A\beta_p$. Our observations indicated up to 1.4 M (8.3%) of added ethanol can be used as a solvent/vehicle without quantitatively affecting $A\beta$ pentamer stability. Higher concentration induced significant destabilization of $A\beta_p$ and eventually resulted in the complete disassembly of $A\beta_p$.

Keywords: amyloid- β ; oligomer; atomic force microscopy; gel electrophoresis; Gaussian fitting

1. Introduction

The generation of the amyloid- β ($A\beta$) peptide is a critical event in the pathogenesis of Alzheimer's disease (AD), the most common type of dementia [1–3]. The $A\beta$ precursor encoded by the amyloid precursor protein gene is cleaved by γ -secretase complex into $A\beta$ peptides of various sizes, among which those of the 40 ($A\beta_{1-40}$) and 42 ($A\beta_{1-42}$) amino acids are the most abundant [4,5]. $A\beta_{1-42}$ is the principal species found in the brain lysates of patients with AD [6–8]. The presence of aggregated $A\beta$ in the form of senile plaques is one of the histopathological hallmarks of AD [2,9], but there is an emerging consensus that the soluble $A\beta_{1-42}$ oligomeric assemblies (dimers, trimers, and small oligomeric assembly but not monomers) are also involved in the development of AD [10–12].

In vitro oligomerization using synthetic $A\beta_{1-42}$ peptides results in preparation consisting of various assemblies (oligomers and fibrils). This heterogeneity, probably due to transient meta-stability and different kinetic pathways [13–16], may jeopardize attempts to

characterize A β_{1-42} oligomeric assemblies. Some A β_{1-42} oligomerization protocols have been shown to result in a preferential assembly generation [12,17]. For instance, Ahmed et al. have shown that when parameters such as temperature, pH, salt, and initial monomer concentration are carefully controlled, then the pentameric conformers are the predominant assembly formed. This could be used to establish a model system to evaluate the ability of chemical compounds to destabilize A β_{1-42} pentameric assemblies (A β p); an essential step towards developing therapeutic strategies targeting the processes of A β_{1-42} assembly/disassembly, opening new avenues for the treatment of AD.

Most chemical compounds with the potential to interact on A β_{1-42} oligomeric assemblies are not soluble in water [18], therefore alcohols and other surface-active agents are needed as the solvent/vehicle. Several alcohols have been shown to effectively disassemble A β_{1-42} oligomeric assemblies by acting on the tertiary and quaternary structures, although the exact molecular mechanism remains unknown [13,19,20]. Other studies have reported the effect of another solvent, dimethyl sulfoxide (DMSO), on the conformation of A β_{1-40} and A β_{1-42} [21,22]. However, the effect of ethanol on already assembled A β_{1-42} oligomers has never been reported, even if ethanol has been shown to prevent A β aggregation and protect cultured cells against both A β -induced cell death and synapse damage [23,24].

In this context, the objective of this study was to determine the highest ethanol concentration that could be used as a solvent/vehicle without affecting A β p stability.

Recent studies are showing that direct observation of real space with sub-nanometer resolution, such as scanning probe microscopy (SPM), is useful for accessing peptides, especially their structures [25,26]. Previously, we used SPM to study A β_{1-42} oligomeric assemblies and showed the diversity of oligomeric conformations in vitro [27]. Although SPM permits accurate visualization of A β_{1-42} oligomeric assemblies, reliable quantification is tedious. Here, we studied the effect of ethanol on A β p conformation using a combination of gel electrophoresis and atomic force microscopy (AFM), one of the SPM, two affordable and available technologies in most routine laboratories. These methods were used to assess quickly and reliably a homogeneous population of A β p (obtained under carefully controlled parameters), and then fulfilled the objective of this study.

2. Results

2.1. Electrophoresis

The reliability of A β_{1-42} oligomerization protocol was examined using polyacrylamide gel electrophoresis (PAGE) in both non-denaturing (native) and denaturing conditions. A β_{1-42} oligomeric assemblies were assessed in non-denaturing conditions using blue-native polyacrylamide gel electrophoresis (BN-PAGE) followed by Coomassie Brilliant Blue (CBB) staining (Figure 1A, ctrl). A β_{1-42} oligomeric assemblies were assessed in denaturing conditions using Tricine-SDS-PAGE, followed by Western blot analysis (Figure 1B, ctrl). In native gels, an intense sharp band with an apparent molecular size slightly above 20 kDa was observed; it was consistent with the expected size for A β p. Faintly stained bands above 146 kDa and a smear between 20 and 146 kDa were also observed. On denaturing gels, oligomers are broken down by SDS, and three bands with apparent molecular sizes of 22.5 kDa, 14 kDa, and lower than 10 kDa were observed (Figure 1B). These bands matched the expected sizes for the A β_{1-42} pentamers, trimers, and monomers. Migration patterns on BN and Tricine-SDS gels were consistent with the results reported previously [17]. This confirmed that A β p was the main product of oligomerization seen on BN-PAGE.

Next, we investigated the effect of various concentrations of ethanol on oligomerized A β_{1-42} . After 3 h of incubation with ethanol (concentration from 0 to 7.2 M), the A β_{1-42} oligomerization status was examined by BN-PAGE (Figure 1A). The migration pattern was essentially similar to the control (without ethanol) for ethanol concentrations of up to 4.8 M; however, the intensity of the 20 kDa band obviously decreased as the ethanol concentration increased (Figure 1A). At the highest ethanol concentration tested (7.2 M), no stained band was visible. Later, densitometric analysis of bands (Figure 6A, white bars) confirmed that the 20 kDa band intensity significantly diminished when the ethanol

concentration increased. These results suggest that ethanol definitely affected the stability of oligomerized $A\beta_{1-42}$.

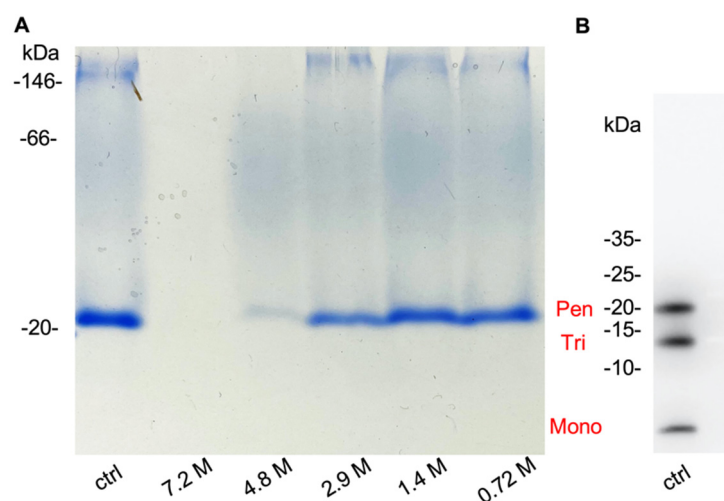


Figure 1. BN-PAGE and Tricine-SDS-PAGE of oligomerized $A\beta_{1-42}$. (A) Blue-native PAGE of oligomerized $A\beta_{1-42}$ incubated with various concentrations of ethanol for 3 h. “ctrl” is incubated with 0 M ethanol. (B) Tricine-SDS-PAGE of oligomerized $A\beta_{1-42}$ solution in same conditions as “ctrl” in (A). Molecular weight markers are shown on the left of each gel image.

2.2. AFM Imaging and Height Distribution

Imaging by AFM was used to resolve the spatial arrangement of oligomerized $A\beta_{1-42}$, in particular their heights. Figure 2a shows AFM resolved images of oligomerized $A\beta_{1-42}$ after 3 h of incubation with various ethanol concentrations. In the control condition, AFM imaging of oligomerized $A\beta_{1-42}$ showed about 10–20 relatively large-size (heights of 1.5–2.9 nm and widths of 1.8–4.6 nm) contrasted-spots (contrasts) per squared micrometers (Figure 2a). The number of large-size contrasts decreased while the number of small-size (heights of 0.5–1.2 nm and widths of 5.0–10 nm) contrasts increased after incubation with increasing ethanol concentrations (Figure 2b–f). These observations are consistent with the BN-PAGE results, showing that ethanol affected the stability of oligomerized $A\beta_{1-42}$. It is noteworthy that AFM imaging clearly showed small contrasted spots after 3 h of incubation with the 7.2 M ethanol concentration, while BN-PAGE did not reveal any signal.

Figure 3 shows the distribution of heights calculated from the AFM contrasts of oligomerized $A\beta_{1-42}$ after incubation with ethanol. For ethanol concentrations ranging from 0 to 1.4 M, the heights of resolved contrasts are distributed up to 6 nm (Figure 3a–c). When the ethanol concentration exceeded 2.9 M (Figure 3d), most contrasts failed under 4 nm in height, and for concentrations over 4.8 M (Figure 3e,f), the resolved contrasts were typically below 2 nm in height with a dense distribution in the range of 0.4–1.8 nm.

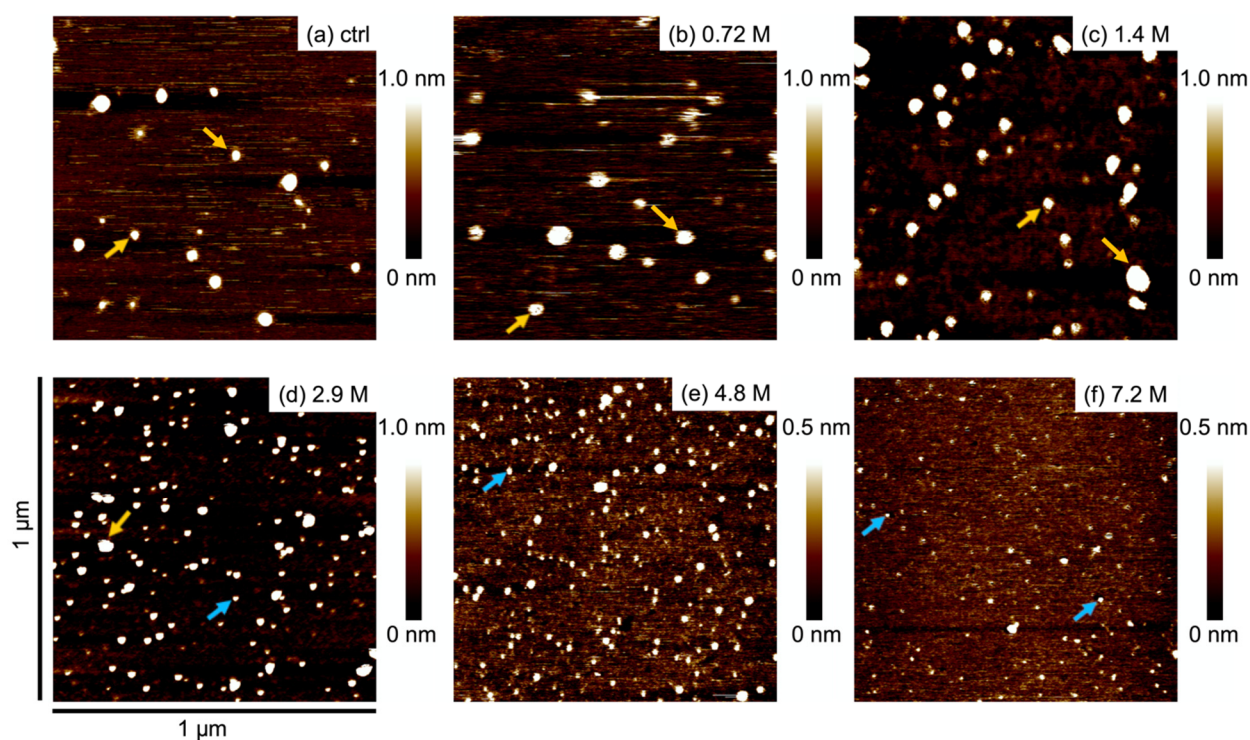


Figure 2. AFM images of oligomerized $A\beta_{1-42}$ incubated with various ethanol concentration for 3 h: (a) control (0 M ethanol), (b) 0.72 M, (c) 1.4 M, (d) 2.9 M, (e) 4.8 M, and (f) 7.2 M. The height contrast is color-coded between 0.0–1.0 nm or 0.0–0.5 nm, as shown in the scale bar, with brighter colors indicating higher particle heights. The height scale was adjusted to a reference position. The yellow and blue arrows show pentamer and monomer, respectively. All AFM images are scaled at 1×1 squared micrometer; scale bars are shown in (d).

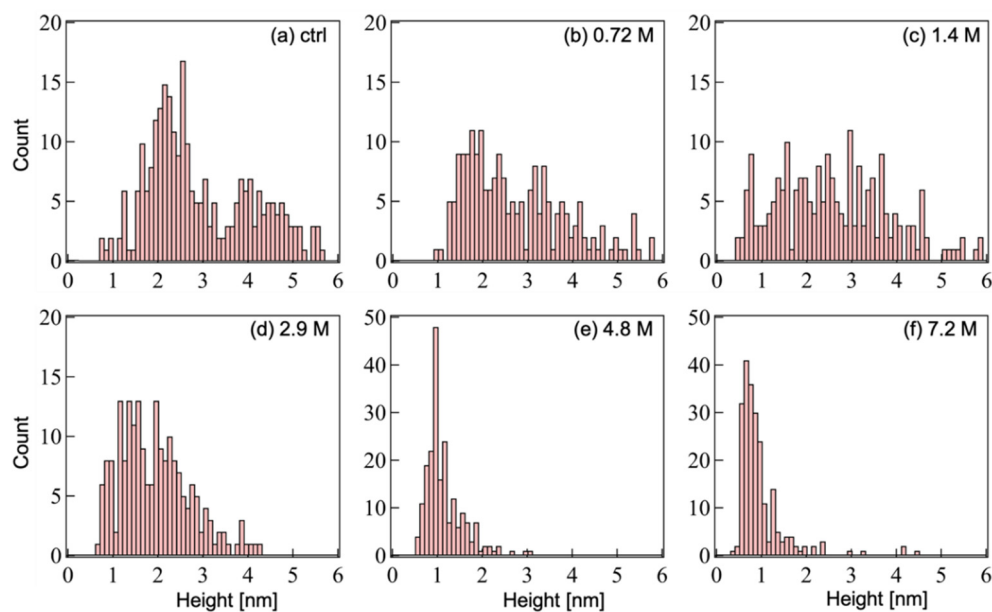


Figure 3. Height histograms of $A\beta_{1-42}$ oligomeric assemblies calculated from the AFM topographic images in Figure 2. Ethanol concentrations: (a) control no ethanol, (b) 0.72 M, (c) 1.4 M, (d) 2.9 M, (e) 4.8 M, and (f) 7.2 M. The number of counted contrasts in each aliquot is more than 200.

2.3. Distribution Height Analysis by Gaussian Fitting

In order to quantify distinct types of A β ₁₋₄₂ oligomeric assemblies based on their height features, we first characterized the signature feature of the monomeric and pentameric assemblies in the height histogram plot of Figure 3. Therefore, we used Gaussian fitting to resolve overlapping heights of peaks, and then we attempted the identification of A β ₁₋₄₂ oligomeric assemblies associated with resolved peaks, as described by Lin et al. [28]. First, Gaussian fitting was applied to the histogram corresponding to the smallest contrasted spots (Figure 3f); this was obtained at the highest ethanol concentration. The resulting Gaussian fitted curve peaked at a value of 0.69 ± 0.26 nm (mean \pm standard deviation; Figure 4A). This corresponded to contrasts with heights of 0.5–1.2 nm and widths of 5.0–10 nm that we categorized as monomers. Next, the same procedure was applied to the histogram of Figure 3a corresponding to the largest and highest contrasted spots observed in control condition (without ethanol), which we assumed to be pentamers in regards to BN-PAGE data. Gaussian fitting resolved two curves peaking at 2.2 ± 0.71 nm and 4.0 ± 0.61 nm (Figure 4B). As suggested by Ahmed et al. [17], we assumed that there were pentamer and double-layered pentamers, respectively. It is important to note that the monomeric height values observed in this study were consistent with those previously reported for the A β ₁₋₄₀ monomer [12,29]. In addition, single layer and double layer A β p height values closely matched those reported in previous studies [17,30–32].

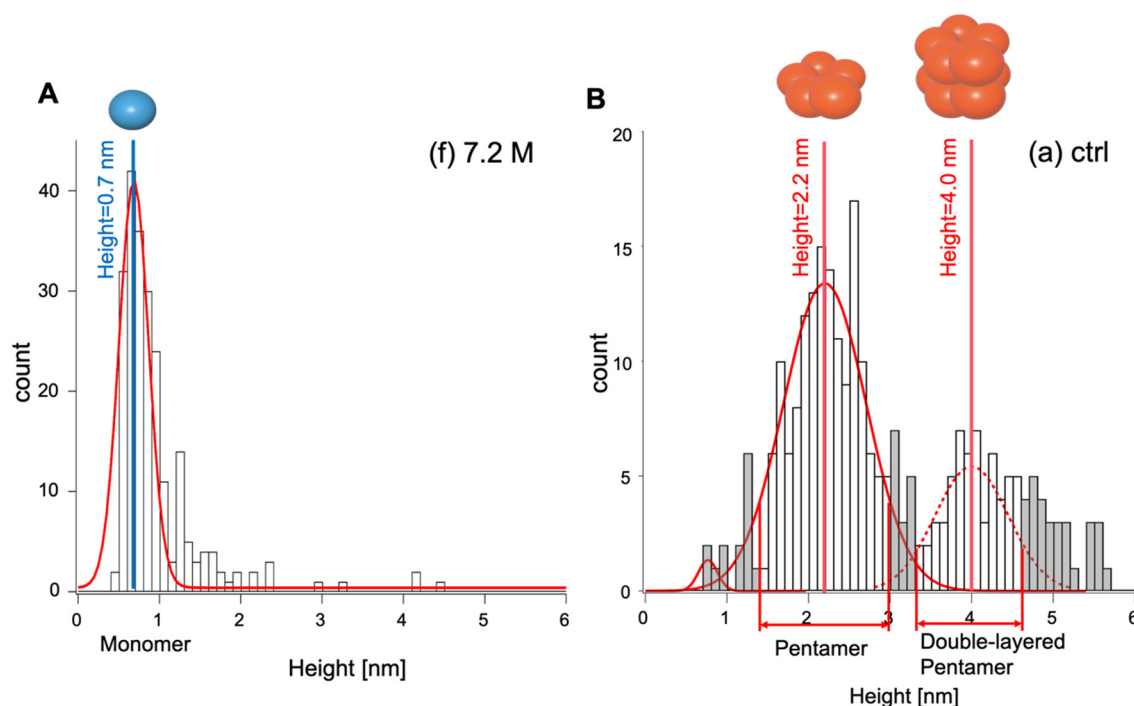


Figure 4. (A) Gaussian fitting for the histogram in Figure 3f. Values of mean and standard deviation are used for the calibration of the monomer. (B) Gaussian fitting applied to the histogram of Figure 3a. Bars in white are included in the pentamer counts.

After Gaussian fitting, this calibration was applied to characterize the monomers, pentamers, and double-layered pentamers peaks histograms; this resulted in Figure 5. Similar to BN-PAGE, A β p forms (single- and double-layered) decreased and monomeric A β ₁₋₄₂ increased when the ethanol concentration increased.

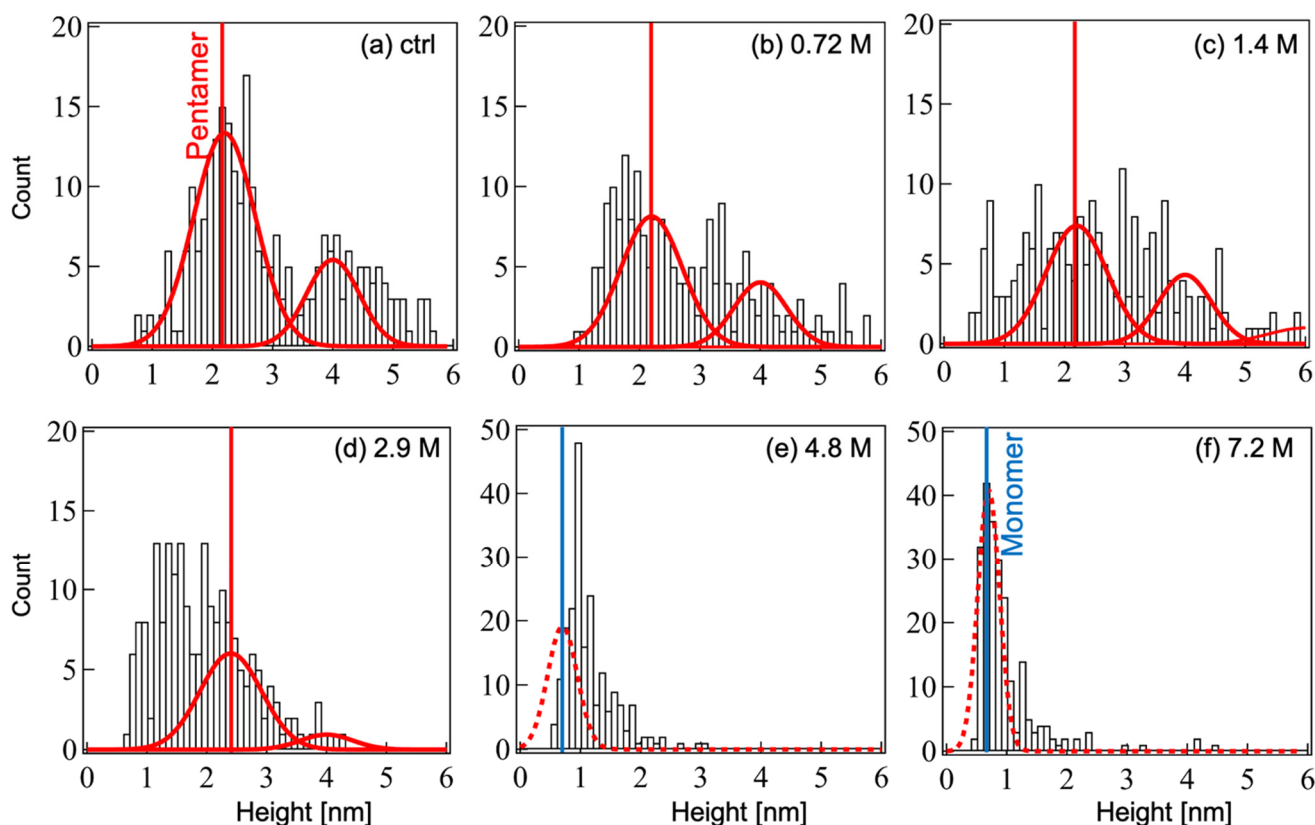


Figure 5. Characterization of $A\beta_{1-42}$ oligomeric assembly by Gaussian fitting and calibration. Ethanol concentration: (a) control (no ethanol), (b) 0.72 M, (c) 1.4 M, (d) 2.9 M, (e) 4.8 M, and (f) 7.2 M. The solid red curves are Gaussian curves with peaks at 2.2 nm and 4.0 nm, and the broken red curves are those at 0.7 nm and 1.4 nm. Blue and red vertical lines are drawn at the values of 0.7 nm and 2.2 nm, respectively.

2.4. Combined AFM and Electrophoresis

The percentage of pentamers from the AFM resolved height was compared to the 20 kDa band intensity observed by BN-PAGE and was measured by software ImageJ (Figure 6A). Pearson's correlation coefficient between the ratio of the number of pentamers in the height histograms and intensities of pentameric bands obtained from three independent BN-PAGE gels was 0.91, indicating a strong correlation between the BN-PAGE and AFM results (Figure 6C).

Figure 6B shows the percentage of monomers counted from the histogram height comprised between $0.69 \text{ nm} \pm 0.26 \text{ nm}$ for all concentrations of ethanol tested. The percentage of monomers was inversely proportional to the percentage of pentamers (Figure 6A, red bars), indicating that as the concentration of ethanol increased, pentamers decreased and monomers increased. This result indicates that ethanol promoted the disassembly of pentamers into monomers.

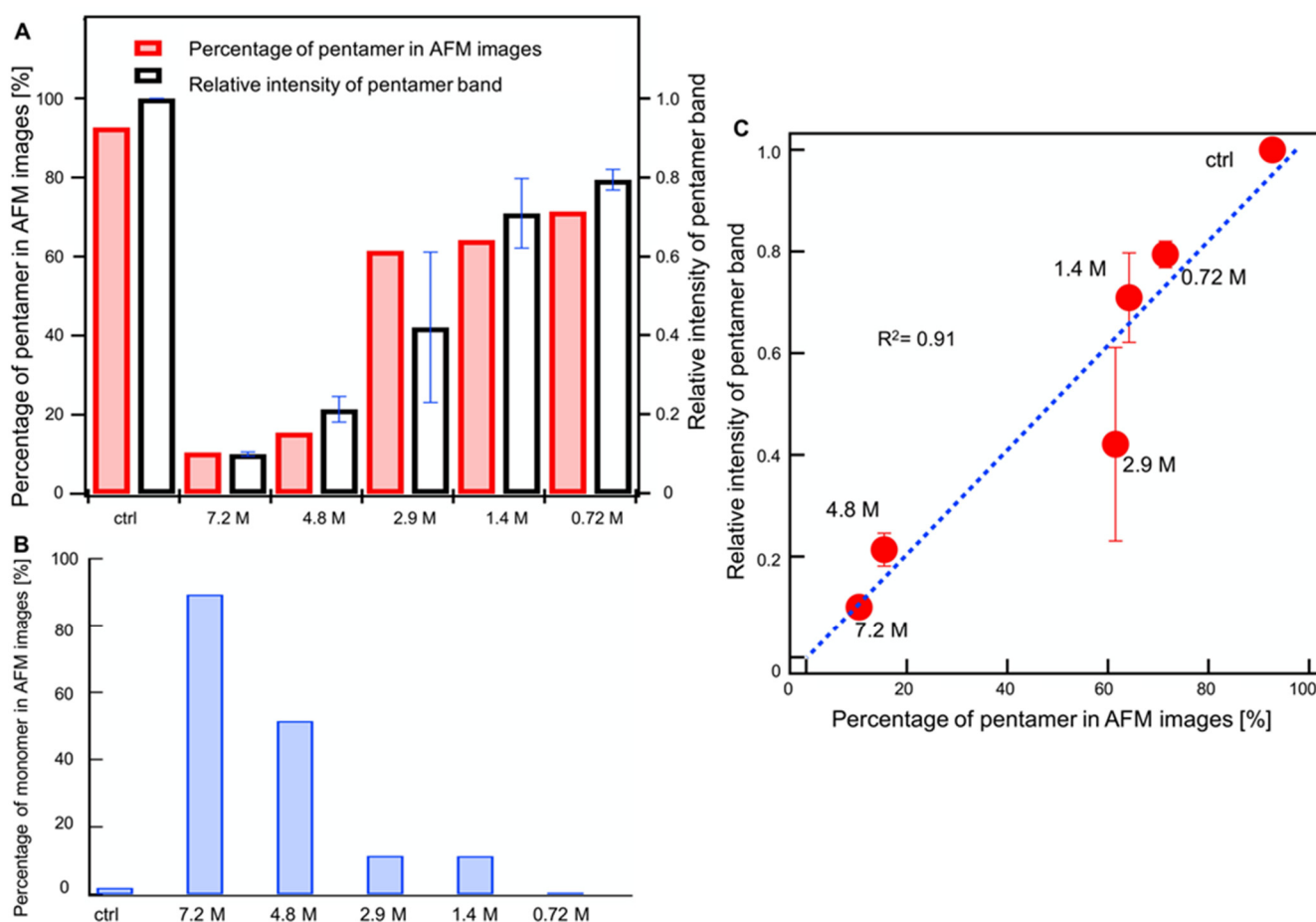


Figure 6. (A) Comparison of the pentameric percentage from AFM images (red bar) with band intensities in BN-PAGE (white bar). The error bar of bands represents the mean \pm standard error of the mean ($n = 3$). (B) Count of monomers in AFM images. (C) Pearson correlation coefficient between the pentameric percentage from AFM images and the average ratio of pentameric band intensity in BN-PAGE.

3. Discussion

In the present study, we assessed the effect of ethanol on A β p. We used a protocol of A β oligomerization, which results in predominant pentameric assembly generation when parameters such as temperature, pH, salt, and initial monomers concentration are carefully controlled [15,33]. A β p generation was confirmed in the present and in previous studies [17,27]. The potential mechanisms liable for the preferential generation of A β p were discussed elsewhere [13,34]. Next, to answer our initial objective to determine which concentration of ethanol can be used as solvent/vehicle without destabilizing A β p assemblies, we investigated the effect of various concentrations of ethanol ranging from 0 to 7.2 M (0~41.4%) on A β p assemblies stability using BN-PAGE and ambient air AFM. Our observations indicated that ethanol concentrations as high as 2.9 M (16.6%) induced significant changes in A β p stability, promoted disassembly, and eventually resulted in the complete disassembly of A β p into monomers at the higher concentration used (i.e., 7.2 M (41.4%)). This is relevant with the fact that A β p assemblies are mostly built on hydrophobic inter- and intramolecular non-covalent interactions [10,35,36], and amphiphilic small molecules like ethanol might affect the stability of A β p by acting as surface-active agents [37–39]. Interestingly, ethanol concentrations up to 1.4 M (8.3%) did not have much effect and could be used as a solvent/vehicle for drugs and chemical compounds to study their effects on A β p stability. In a previous study, Ormeno et al. [23] reported that an ethanol concentration as low as 10 mM was able to prevent the build-up of A β ₁₋₄₀ aggre-

gates, an almost 100 times lower ethanol concentration than what was required here to disassemble A β p. This indicates that interfering with A β oligomerization required a lower ethanol concentration than that needed to disassemble the already build up A β oligomeric assembly. Finally, a study using DMSO as a solvent for A β_{1-42} has shown that DMSO up to 10% does not affect A β_{1-42} oligomeric assembly stability; however, it has also been reported that DMSO may oxidate A β_{1-42} methionine [40].

The above finding answered our initial question, however, several additional observations deserved further discussion. We used BN-PAGE and ambient air AFM to investigate the effect of ethanol on A β p assembly—these are two affordable technologies that are relatively easy to set up in a routine biochemical laboratory. Interpretations of individual BN-PAGE and AFM datasets showed limitations, but their combination permitted a reliable quantitative assessment of A β p stability. BN-PAGE followed by Coomassie blue staining has been previously used to quantify A β p pentamers [17,27]. On our hand, we observed that BN-PAGE was unable to reveal low molecular weight A β assembly (i.e., monomers, dimer, trimer, and tetramer). The reason for this shortcoming is unclear; it could be due to the lack of sensitivity of Coomassie blue staining, the lack of resolution of the gel system used, or both [41]. On the other hand, AFM was very effective for a quick visual assessment. It could also identify A β oligomeric forms after cross-sectional height analysis by Gaussian fitting, and calibration using monomeric A β and A β p profiles. With this original approach, we were able to follow A β p disassembly when the ethanol concentration increased. The correlation between band intensity by BN-PAGE and pentamers count by AFM demonstrated that in our experimental setting, BN-PAGE could be used to quickly and reliably quantify A β p. The combination of AFM and BN-PAGE may be an alternative approach to the actual methodologies for relating the molecular weight of peptides to their size and spatial organization, being able to quickly estimate their relative amounts [42].

The histogram of the height distribution of A β p in the absence of ethanol showed two peaks. Based on previous observations, we interpreted them as single-layered A β p (Figure 4B left peak red line) and double-layered A β p (Figure 4B right peak red line) [17,27,31]. In contrast, the BN-PAGE analysis showed only a single band with a molecular size corresponding to that of a single-layered pentamer. This difference suggests either that double-layered A β p is an artifact generated during processing the sample for AFM or that double-layered A β p breaks down into single-layered A β p during BN-PAGE migration. It was previously reported that during sample preparation for AFM observation, A β_{1-42} dispersed on mica could form oligomers and fibrils due to the presence of residual water [30,43,44]. In our experimental setting, when A β monomers were incubated for a short time, then only single-layered A β p were observed using AFM (Supplementary Figure S1). This indicates that double-layered A β p was not an artifact in our preparation. Alternatively, dyes have been shown to break down amyloid fibrils, suggesting that CBB (present in the loading buffer of BN-PAGE) may break down double-layered A β p into single-layered A β p [45]. Noteworthy, we observed that the actual best correlation between band intensity after BN-PAGE and pentamers count after AFM were obtained when pentamers count included the number of single-layered A β p plus twice the number double-layered A β p. Attempts to correlate BN-PAGE band intensity with the count number of single-layered A β p only resulted in a weaker correlation (Supplementary Figure S2). This assumption suggests that the interactions keeping A β p stacked together to form double-layered A β p are weaker than the interactions making the A β p assembly. This supports the computer simulation predicting that A β p models can be stacked to form a loosely packed decameric A β (double-layered A β p) through a small number of hydrophobic interactions [31].

In line with the previous assumption, we described a drastic decrease in the number of double-layered pentamers in the presence of ethanol concentrations as high as 2.9 M (16.6%), then complete disassembly of A β p into monomeric A β at the highest ethanol concentration used (i.e., 7.2 M (41.4%)). It was tempting to reconstitute the sequence of double-layered A β p break down and A β p disassembly, however, it appears very complex. Many intermediate heights between double-layered A β p and single-layered heights sug-

gested that a molecular intermediate existed, maybe mixed double-layered with A β p and another A β form (monomer, dimer, trimer, and tetramers). While we were able to calibrate the A β p and A β monomer height peaks, other heights were difficult to reliably identify; as a result, the sequence of events leading to A β p disassembly was not resolved and will require further studies.

In conclusion, we found that ethanol concentrations up to 1.4 M (8.3%) have no significant effect on single-layered A β p stability and can be used as a solvent/vehicle for drugs and chemical compounds. We showed that a combination of AFM and BN-PAGE, two technologies readily available and affordable, might provide new insight facilitating both qualitative and quantitative assessment of the A β oligomeric forms. Interestingly, we showed that ethanol concentrations as high as 2.9 M (16.6%) were able to disassemble already formed A β p assemblies.

4. Materials and Methods

4.1. Materials

Amyloid- β_{1-42} (human, Trifluoroacetate) was purchased from Peptide Institute (Osaka, Japan); UV/mass spectrometry high-performance liquid chromatography and amino acid analysis provided by the maker indicated 95% purity and confirmed the identity of the peptides. Low-binding microtubes and tips were used for all of the procedures involving peptides. All of the reagents were purchased from Nacalai Tesque (Kyoto, Japan) unless otherwise indicated. Ethanol (99.5%) was converted into moles from the indicated values according to the International Alcohol Table based on the International Organization of Legal Metrology (https://www.oiml.org/en/files/pdf_r/r022-e75.pdf) (accessed on 12 December 2021).

4.2. A β Oligomer Sample Preparation

Amyloid- β oligomers were generated according to the procedure described by Ahmed et al. [17]. First, A β_{1-42} monomers were prepared by dissolving peptides, with gentle pipetting, in hexafluoroisopropanol (HFIP, Fujifilm, Osaka, Japan) to a final concentration of 3.3 mg/ml. The resulting solution was transferred into a microtube, and the solvent was removed by vacuum freeze-drying. Lyophilized A β_{1-42} monomer preparation was dissolved in 1020 μ L of a buffer solution consisting of 3.5% of 0.1 M NaOH (aqueous solution) in a 0.05 M phosphate buffer (pH 7.4) containing 0.05 M NaCl (Fujifilm, Osaka, Japan). The resulting 0.12 mM A β_{1-42} solution was aliquoted in six equal parts into microtubes and was incubated for 3 h at 4 °C. Next, each aliquot was incubated for another 3 h at 4 °C with various ethanol concentrations (Table 1). The A β_{1-42} concentration was adjusted to 72 mM in each tube by adding a cold buffer solution for a final volume of 290 μ L. For AFM, the samples were used immediately; for BN-PAGE and Tricine-SDS-PAGE, all of the aliquots were quickly frozen in liquid nitrogen and stored at –80 °C until use.

Table 1. Molar amounts of A β_{1-42} and ethanol in the samples. The ratio of A β_{1-42} /ethanol is defined as the molar ratio. A β_{1-42} solution is considered uniform by sufficient stirring and dispersion, and the molar amount is calculated assuming that after HFIP treatment, the content of vials is exclusively monomers.

A β_{1-42} Peptide [nmol]	21	21	21	21	21	21
Ethanol [μ L]	0 (ctrl)	120	80	48	24	12
Ethanol [M]	0	7.2	4.8	2.9	1.4	0.72
Ethanol [%]	0	41.4	27.6	16.6	8.3	4.1
Molar Ratio (A β_{1-42} /ethanol)	-	1.0×10^{-5}	1.5×10^{-5}	2.5×10^{-5}	5.0×10^{-5}	1.0×10^{-4}

4.3. Electrophoresis

Blue-native PAGE was carried out as described by Schagger and von Jagow [46], with slight modifications. We introduced two modifications to the original BN-PAGE protocol [45]—the use of 10–20% gradient gel and the addition of Coomassie blue into the loading buffer. It improved the sharpness of the bands, resulting in more accurate quantification and molecular weight determination. Gradient mini-gels (9 × 7 cm) were prepared using acrylamide/bis-acrylamide mixed solution (37.5:1; Fujifilm, Osaka, Japan) in 300 mM Bis-tris buffer (pH 7.0) containing 400 mM 6-aminocaproic acid. The stacking layer consisted of 4% acrylamide/bis-acrylamide mixed solution in the same buffer as above. Immediately after thawing, 50 µL of AβOs solutions were added to 25 µL Native PAGE sample buffer (Thermo Fisher Scientific, Ann Arbor MI, USA) containing 0.05% CBB G250. Then, 10 µL was loaded onto the 10–20% gradient gel and it was electrophoresed for 60 min at 70 V followed by 50 min at 200 V; cathode and anode running buffers were used (NativePAGE™ Cathode Buffer Additive and NativePAGE™ Running Buffer, Thermo Fisher Scientific, Ann Arbor, MI, USA). Native-Mark unstained protein standards (Thermo Fisher Scientific, Ann Arbor, MI, USA) were used as the molecular weight markers. After electrophoresis, gels were stained with Coomassie blue dye (rapid stain CBB kit, Nacalai-Tesque, Kyoto, Japan) for 1–3 days and were washed extensively with Milli-Q water to remove the background dark blue color. The gels were set on a LED lightbox (Konica, Tokyo Japan), and the images were acquired using an iPhone (Apple, Cupertino, CA, USA). The images were adjusted for contrast and luminosity only, and the band intensity was quantified using ImageJ [47,48] and calculated as relative values compared with the control lane (no ethanol).

Tricine-SDS-PAGE was performed following the method described by Schagger [49]. Immediately after thawing, 10 µL AβOs solutions were mixed with 50 µL non-reducing sample buffer solution (Fujifilm, Osaka, Japan) and loaded onto Novex 10–20% Tricine gels (Thermo Fisher Scientific, Ann Arbor, MI, USA). Nacalai Ladder-one plus stained protein standards were used as the molecular weight markers. Gel electrophoresis was carried out for 15 min at 60 V, for 60 min at 90 V, and for 60 min at 80 V using running cathode (0.1 M Tris-tricine and 1% SDS, pH 8.25) and anode (0.1 M Tris, pH 8.9) buffers. Separated peptides were transferred onto a PVDF membrane for Western blot analysis, as previously described [50]. The membrane was blocked in 5% skimmed milk dissolved in Tris-buffered saline with Tween 20 (TBST; 20 mM Tris-HCl, pH 7.6, 150 mM NaCl, 0.1% Tween 20) for 30 min. The blocked membrane was incubated overnight at room temperature with a 100 ng/ml anti-Aβ₁₋₁₆ antibody in TBST containing 1% skimmed milk. Anti-Aβ₁₋₁₆ is a purified mouse monoclonal IgG1, κ antibody (Biolegend, San Diego, CA, USA; clone 6E10, CAT#803001, LOT#B247600), which has been validated for Western blot application. After incubation, the membrane was washed 3 × 10 min in TBST, then incubated for 1 h at room temperature with secondary peroxidase-labeled rabbit anti-mouse IgG(H+L) antibody (Jackson ImmunoResearch Laboratories, West Grove, PA, USA) diluted 1:20,000 in TBST. After further washes in TBST, the membrane was incubated for 1 min with a Chemi-Lumi One Super chemiluminescent substrate. Images were acquired using FUSION solo-S system (Vilber-Lourmat, Collégien, France), with settings to ensure an optimal dynamic range. The images in the figures were adjusted for contrast and luminosity only.

4.4. AFM Observations

Immediately after incubation with ethanol, aliquots of AβOs solution were diluted 200-times with Milli-Q, and 8 µL were dispersed onto a freshly cleaved mica disc (V-1 Grade 9.5 nm φ × 0.15 nm, Alliance Biosystems Co., Ltd., Osaka, Japan), which we confirmed as being ideally flat (height < ±0.3 nm). This procedure was performed to reduce the risk that the buffer solution changes the hydration landscape of Aβ₁₋₄₂ and that potassium carbonate crystallites can be present on mica surface [51,52]. After drying in an antistatic case at 4 °C in a dry environment, observations were carried out using an AFM Innova system (Bruker, Billerica, MA, USA), operating in the air under ambient humidity and room

temperature conditions. Mica discs were examined with AFM using the tapping mode. The resonant frequency was about 110 kHz. Areas of 1×1 micrometer and 512×512 pixels were acquired using software NanoDrive (v8.02, Bruker, Billerica, MA, USA) by scanning at 0.7 Hz. A silicon cantilever (RTESP-150, Bruker, Billerica, MA, USA) with a spring constant of 5 Nm/s (nominal value) and a tip radius of ~ 12 nm was used. Minimal resolutions in the x-, y-, and z-axis (height) were 0.1 nm and 0.1 nm, respectively.

4.5. Image and Histogram Analysis

Images obtained by AFM were analyzed with Gwyddion software (<http://gwyddion.net/> version 2.56 (accessed on 12 January 2022)) [53]. To derive the true height of $A\beta_{1-42}$ oligomeric assemblies by eliminating the effects of surface corrugation and scan noises, a cross-sectional analysis was conducted to obtain the actual height of the $A\beta_{1-42}$ oligomeric assemblies in the AFM images fitted by Gaussian using Igor Pro 8 (HULINKS Inc., Tokyo, Japan) [54]. Several AFM images were acquired to generate the height histograms [25,55,56].

Gaussian fitting analyses for height histograms were based on the work of Lin, Y.C., and were also calculated using Igor Pro 8 (HULINKS Inc., Tokyo, Japan) [28]. To characterize the heights of the $A\beta_{1-42}$ oligomeric assemblies, normalized height distributions were fitted by two or more Gaussian functions (Supplementary Figure S3).

For the correlation study, the total number of pentamers interpreted from the histograms was counted based on the pentamer height size of 1.5–2.9 nm and 3.4–4.6 nm for single and double-layered pentamers, respectively. The total population of pentamers was counted as the number contrast in the height range of 1.5–2.9 nm plus twice the number in the height range of 3.4–4.6 nm (double-layered pentamers).

Supplementary Materials: The following supporting information can be downloaded at: <https://www.mdpi.com/article/10.3390/ijms23020889/s1>.

Author Contributions: Conceptualization, H.T. and N.N.; methodology, A.M., J.-P.B. and N.N.; formal analysis, A.M. and N.N.; investigation, A.M., J.-P.B., T.K., H.S., A.N., T.T., T.I. and Y.N.; resources, Y.N., J.-P.B. and Y.M.; data curation, A.M. and N.N.; writing—original draft preparation, A.M. and N.N.; writing—review and editing, A.M., H.T., N.N. and Y.M.; visualization, A.M. and J.-P.B.; supervision, N.N.; funding acquisition, N.N. The manuscript was written through the contributions of all of the authors. All authors have read and agreed to the published version of the manuscript.

Funding: This work was supported by a Grant-in-Aid for Scientific Research C (19K05207) from JSPS KAKENHI, Japan.

Institutional Review Board Statement: Not applicable.

Informed Consent Statement: Not applicable.

Data Availability Statement: The data presented in this study are available upon request from the corresponding authors.

Acknowledgments: We would also like to express our gratitude to Ikuo Tooyama, Takako Hirata, and Yoshio Furusho of Shiga University of Medical Science, and Eri Chatani and Akihiko Tsuda of Kobe University for providing suggestions on the research.

Conflicts of Interest: The authors declare no conflict of interest.

References

1. Harper, J.D.; Wong, S.S.; Lieber, C.M.; Lansbury, P.T. Assembly of $A\beta$ Amyloid Protofibrils: An in Vitro Model for a Possible Early Event in Alzheimer's Disease. *Biochemistry* **1999**, *38*, 8972–8980. [[CrossRef](#)]
2. Lacor, P.N.; Buniel, M.C.; Furlow, P.W.; Clemente, A.S.; Velasco, P.T.; Wood, M.; Viola, K.L.; Klein, W.L. $A\beta$ Oligomer-Induced Aberrations in Synapse Composition, Shape, and Density Provide a Molecular Basis for Loss of Connectivity in Alzheimer's Disease. *J. Neurosci.* **2007**, *27*, 796–807. [[CrossRef](#)]
3. Selkoe, D.J.; Hardy, J. The Amyloid Hypothesis of Alzheimer's Disease at 25 Years. *EMBO Mol. Med.* **2016**, *8*, 595–608. [[CrossRef](#)] [[PubMed](#)]

4. Lammich, S.; Kojro, E.; Postina, R.; Gilbert, S.; Pfeiffer, R.; Jasionowski, M.; Haass, C.; Fahrenholz, F. Constitutive and Regulated α -Secretase Cleavage of Alzheimer's Amyloid Precursor Protein by a Disintegrin Metalloprotease. *Proc. Natl. Acad. Sci. USA* **1999**, *96*, 3922–3927. [[CrossRef](#)]
5. Ye, I.Y.; Bassit, B.; Zhu, L.; Yang, X.; Wang, C.; Li, Y.M. γ -Secretase Substrate Concentration Modulates the A β 42/A β 40 Ratio: Implications for Alzheimer Disease. *J. Biol. Chem.* **2007**, *282*, 23639–23644. [[CrossRef](#)]
6. Iwatsubo, T.; Odaka, A.; Suzuki, N.; Mizusawa, H.; Nukina, N.; Ihara, Y. Visualization of A β 42(43) and A β 40 in Senile Plaques with End-Specific A β Monoclonals: Evidence That an Initially Deposited Species Is A β 42(43). *Neuron* **1994**, *13*, 45–53. [[CrossRef](#)]
7. Viola, K.L.; Klein, W.L.; Klein, W.L. Amyloid β Oligomers in Alzheimer's Disease Pathogenesis, Treatment, and Diagnosis. *Acta Neuropathol.* **2015**, *3*, 183–206. [[CrossRef](#)]
8. Walsh, D.M.; Selkoe, D.J. Deciphering the Molecular Basis of Memory Failure in Alzheimer's Disease. *Neuron* **2004**, *44*, 181–193. [[CrossRef](#)] [[PubMed](#)]
9. Sayre, L.M.; Perry, G.; Harris, P.L.R.; Liu, Y.; Schubert, K.A.; Smith, M.A. In Situ Oxidative Catalysis by Neurofibrillary Tangles and Senile Plaques in Alzheimer's Disease: A Central Role for Bound Transition Metals. *J. Neurochem.* **2000**, *74*, 270–279. [[CrossRef](#)] [[PubMed](#)]
10. Campioni, S.; Mannini, B.; Zampagni, M.; Pensalfini, A.; Parrini, C.; Evangelisti, E.; Relini, A.; Stefani, M.; Dobson, C.M.; Cecchi, C.; et al. A Causative Link between the Structure of Aberrant Protein Oligomers and Their Toxicity. *Nat. Chem. Biol.* **2010**, *6*, 140–147. [[CrossRef](#)]
11. Lambert, M.P.; Barlow, A.K.; Chromy, B.A.; Edwards, C.; Freed, R.; Liosatos, M.; Morgan, T.E.; Rozovsky, I.; Trommer, B.; Viola, K.L.; et al. Diffusible, Nonfibrillar Ligands Derived from A β 1–42 Are Potent Central Nervous System Neurotoxins. *Proc. Natl. Acad. Sci. USA* **1998**, *95*, 6448–6453. [[CrossRef](#)] [[PubMed](#)]
12. De, S.; Wirthensohn, D.C.; Flagmeier, P.; Hughes, C.; Aprile, F.A.; Ruggeri, F.S.; Whiten, D.R.; Emin, D.; Xia, Z.; Varela, J.A.; et al. Different Soluble Aggregates of A β 42 Can Give Rise to Cellular Toxicity through Different Mechanisms. *Nat. Commun.* **2019**, *10*. [[CrossRef](#)] [[PubMed](#)]
13. Barz, B.; Liao, Q.; Strodel, B. Pathways of Amyloid- β Aggregation Depend on Oligomer Shape. *J. Am. Chem. Soc.* **2018**, *140*, 319–327. [[CrossRef](#)]
14. Michaels, T.C.T.; Šarić, A.; Curk, S.; Bernfur, K.; Arosio, P.; Meisl, G.; Dear, A.J.; Cohen, S.I.A.; Dobson, C.M.; Vendruscolo, M.; et al. Dynamics of Oligomer Populations Formed during the Aggregation of Alzheimer's A β 42 Peptide. *Nat. Chem.* **2020**, *12*, 445–451. [[CrossRef](#)] [[PubMed](#)]
15. Jarvet, J.; Damberg, P.; Bodell, K.; Göran Eriksson, L.E.; Gräslund, A. Reversible Random Coil to β -Sheet Transition and the Early Stage of Aggregation of the A β (12–28) Fragment from the Alzheimer Peptide. *J. Am. Chem. Soc.* **2000**, *122*, 4261–4268. [[CrossRef](#)]
16. Matsumura, S.; Shinoda, K.; Yamada, M.; Yokojima, S.; Inoue, M.; Ohnishi, T.; Shimada, T.; Kikuchi, K.; Masui, D.; Hashimoto, S.; et al. Two Distinct Amyloid β -Protein (A β) Assembly Pathways Leading to Oligomers and Fibrils Identified by Combined Fluorescence Correlation Spectroscopy, Morphology, and Toxicity Analyses. *J. Biol. Chem.* **2011**, *286*, 11555–11562. [[CrossRef](#)]
17. Ahmed, M.; Davis, J.; Aucoin, D.; Sato, T.; Ahuja, S.; Aimoto, S.; Elliott, J.I.; Van Nostrand, W.E.; Smith, S.O. Structural conversion of neurotoxic amyloid- β 1–42 oligomers to fibrils. *Nat. Struct. Mol. Biol.* **2010**, *17*, 561–567. [[CrossRef](#)]
18. Pagano, K.; Tomaselli, S.; Molinari, H.; Ragona, L. Natural Compounds as Inhibitors of A β Peptide Aggregation: Chemical Requirements and Molecular Mechanisms. *Front Neurosci.* **2020**, *14*, 619667. [[CrossRef](#)]
19. Hong, D.P.; Hoshino, M.; Kuboi, R.; Goto, Y. Clustering of Fluorine-Substituted Alcohols as a Factor Responsible for Their Marked Effects on Proteins and Peptides. *J. Am. Chem. Soc.* **1999**, *121*, 8427–8433. [[CrossRef](#)]
20. Stine, W.B.; Dahlgren, K.N.; Krafft, G.A.; LaDu, M.J. In Vitro Characterization of Conditions for Amyloid- β Peptide Oligomerization and Fibrillogenesis. *J. Biol. Chem.* **2003**, *278*, 11612–11622. [[CrossRef](#)]
21. Laurents, D.V.; Pantoja-Uceda, D.; López, L.C.; Carrodegua, J.A.; Mompeán, M.; Jiménez, M.; Sancho, J. DMSO Affects A β 1–40's Conformation and Interactions with Aggregation Inhibitors as Revealed by NMR. *RSC Adv.* **2015**, *5*, 69761–69764. [[CrossRef](#)]
22. Shen, C.L.; Murphy, R.M. Solvent Effects on Self-Assembly of Beta-Amyloid Peptide. *Biophys. J.* **1995**, *69*, 640–651. [[CrossRef](#)]
23. Ormeño, D.; Romero, F.; López-Fenner, J.; Avila, Á.; Martínez-Torres, A.; Parodi, J. Ethanol Reduces Amyloid Aggregation In Vitro and Prevents Toxicity in Cell Lines. *Arch. Med. Res.* **2013**, *44*, 1–7. [[CrossRef](#)] [[PubMed](#)]
24. Bate, C.; Williams, A. Ethanol Protects Cultured Neurons against Amyloid- β and α -Synuclein-Induced Synapse Damage. *Neuropharmacology* **2011**, *61*, 1406–1412. [[CrossRef](#)]
25. Simone Ruggeri, F.; Habchi, J.; Cerreta, A.; Dietler, G. AFM-Based Single Molecule Techniques: Unraveling the Amyloid Pathogenic Species. *Curr. Pharm. Des.* **2016**, *22*, 3950–3970. [[CrossRef](#)]
26. Zorbas, V.; Ortiz-Acevedo, A.; Dalton, A.B.; Yoshida, M.M.; Dieckmann, G.R.; Draper, R.K.; Baughman, R.H.; Jose-Yacaman, M.; Musselman, I.H. Preparation and Characterization of Individual Peptide-Wrapped Single-Walled Carbon Nanotubes. *J. Am. Chem. Soc.* **2004**, *126*, 7222–7227. [[CrossRef](#)] [[PubMed](#)]
27. Naruse, N.; Satooka, H.; Todo, K.; Nakanishi, A.; Taguchi, H.; Mera, Y. Oligomers imaging of amyloid- β 1–42 by scanning tunneling microscopy. *Jpn. J. Appl. Phys.* **2019**, *58*, S11B30. [[CrossRef](#)]
28. Lin, Y.C.; Komatsu, H.; Ma, J.; Axelsen, P.H.; Fakhraai, Z. Quantitative Analysis of Amyloid Polymorphism Using Height Histograms to Correct for Tip Convolution Effects in Atomic Force Microscopy Imaging. *RSC Adv.* **2016**, *6*, 114286–114295. [[CrossRef](#)]

29. Losic, D.; Martin, L.L.; Mechler, A.; Aguilar, M.I.; Small, D.H. High Resolution Scanning Tunnelling Microscopy of the β -Amyloid Protein (A β 1-40) of Alzheimer's Disease Suggests a Novel Mechanism of Oligomer Assembly. *J. Struct. Biol.* **2006**, *155*, 104–110. [[CrossRef](#)]
30. Mastrangelo, I.A.; Ahmed, M.; Sato, T.; Liu, W.; Wang, C.; Hough, P.; Smith, S.O. High-Resolution Atomic Force Microscopy of Soluble A β 42 Oligomers. *J. Mol. Biol.* **2006**, *358*, 106–119. [[CrossRef](#)]
31. Tran, L.; Basdevant, N.; Prévost, C.; Ha-Duong, T. Structure of Ring-Shaped A β 42 Oligomers Determined by Conformational Selection. *Sci. Rep.* **2016**, *6*, 21429. [[CrossRef](#)] [[PubMed](#)]
32. Lopes, P.; Xu, M.; Zhang, M.; Zhou, T.; Yang, Y.; Wang, C.; Ferapontova, E.E. Direct Electrochemical and AFM Detection of Amyloid- β Peptide Aggregation on Basal Plane HOPG. *Nanoscale* **2014**, *6*, 7853–7857. [[CrossRef](#)]
33. Murphy, M.P.; Levine, H. Alzheimer's Disease and the Amyloid- β Peptide. *J. Alzheimer's Dis.* **2010**, *19*, 311–323. [[CrossRef](#)] [[PubMed](#)]
34. Marina, G.B.; Kirkitadze, D.; Lomakin, A.; Vollers, S.S.; Benedek, G.B.; Teplow, D.B. Amyloid β -Protein (A β) Assembly: A β 40 and A β 42 Oligomerize through Distinct Pathways. *Proc. Natl. Acad. Sci. USA* **2003**, *100*, 330–335. [[CrossRef](#)]
35. Ladiwala, A.R.A.; Litt, J.; Kane, R.S.; Aucoin, D.S.; Smith, S.O.; Ranjan, S.; Davis, J.; Van Nostrand, W.E.; Tessier, P.M. Conformational Differences between Two Amyloid β oligomers of Similar Size and Dissimilar Toxicity. *J. Biol. Chem.* **2012**, *287*, 24765–24773. [[CrossRef](#)]
36. Jana, A.K.; Sengupta, N. A β Self-Association and Adsorption on a Hydrophobic Nanosurface: Competitive Effects and the Detection of Small Oligomers via Electrical Response. *Soft Matter* **2015**, *11*, 269–279. [[CrossRef](#)]
37. Thomas, P.D.; Dill, K.A. Local and Nonlocal Interactions in Globular Proteins and Mechanisms of Alcohol Denaturation. *Protein Sci.* **1993**, *2*, 2050–2065. [[CrossRef](#)]
38. Liu, Y.; Bolen, D.W. The Peptide Backbone Plays a Dominant Role in Protein Stabilization by Naturally Occurring Osmolytes. *Biochemistry* **1995**, *34*, 12884–12891. [[CrossRef](#)]
39. Hirota, N.; Mizuno, K.; Goto, Y. Group Additive Contributions to the Alcohol-Induced α -Helix Formation of Melittin: Implication for the Mechanism of the Alcohol Effects on Proteins. *J. Mol. Biol.* **1998**, *275*, 365–378. [[CrossRef](#)]
40. Bitan, G.; Tarus, B.; Vollers, S.S.; Lashuel, H.A.; Condron, M.M.; Straub, J.E.; Teplow, D.B. A Molecular Switch in Amyloid Assembly: Met 35 and Amyloid β -Protein Oligomerization. *J. Am. Chem. Soc.* **2003**, *125*, 15359–15365. [[CrossRef](#)] [[PubMed](#)]
41. Jovin, T.M. Multiphasic Zone Electrophoresis. II. Design of Integrated Discontinuous Buffer Systems for Analytical and Preparative Fractionation. *Biochemistry* **1973**, *12*, 879–890. [[CrossRef](#)] [[PubMed](#)]
42. Erickson, H.P. Size and Shape of Protein Molecules at the Nanometer Level Determined by Sedimentation, Gel Filtration, and Electron Microscopy. *Biol. Proced. Online* **2009**, *11*, 32. [[CrossRef](#)] [[PubMed](#)]
43. Nirmalraj, P.N.; List, J.; Battacharya, S.; Howe, G.; Xu, L.; Thompson, D.; Mayer, M. Complete Aggregation Pathway of Amyloid β (1-40) and (1-42) Resolved on an Atomically Clean Interface. *Sci. Adv.* **2020**, *6*, eaaz6014. [[CrossRef](#)]
44. Meisl, G.; Yang, X.; Hellstrand, E.; Frohm, B.; Kirkegaard, J.B.; Cohen, S.I.A.; Dobson, C.M.; Linse, S.; Knowles, T.P.J. Differences in Nucleation Behavior Underlie the Contrasting Aggregation Kinetics of the A β 40 and A β 42 Peptides. *Proc. Natl. Acad. Sci. USA* **2014**, *111*, 9384–9389. [[CrossRef](#)] [[PubMed](#)]
45. How, S.-C.; Hsu, W.-T.; Tseng, C.-P.; Lo, C.-H.; Chou, W.-L.; Wang, S.S.-S. Brilliant Blue R Dye Is Capable of Suppressing Amyloid Fibril Formation of Lysozyme. *J. Biomol. Struct. Dyn.* **2018**, *36*, 3420–3433. [[CrossRef](#)]
46. Schagger, H.; von Jagow, G. Blue Native Electrophoresis for Isolation of Membrane Protein Complexes in Enzymatically Active Form. *Anal. Biochem.* **1991**, *199*, 223–231. [[CrossRef](#)]
47. Gassmann, M.; Grenacher, B.; Rohde, B.; Vogel, J. Quantifying Western Blots: Pitfalls of Densitometry. *Electrophoresis* **2009**, *30*, 1845–1855. [[CrossRef](#)]
48. Gallo-Oller, G.; Ordoñez, R.; Dotor, J. A New Background Subtraction Method for Western Blot Densitometry Band Quantification through Image Analysis Software. *J. Immunol. Methods* **2018**, *457*, 1–5. [[CrossRef](#)] [[PubMed](#)]
49. Schagger, H. Tricine-SDS-PAGE. *Nat. Protoc.* **2006**, *1*, 16–22. [[CrossRef](#)]
50. Bellier, J.P.; Kimura, H. Acetylcholine Synthesis by Choline Acetyltransferase of a Peripheral Type as Demonstrated in Adult Rat Dorsal Root Ganglion. *J. Neurochem.* **2007**, *101*, 1607–1618. [[CrossRef](#)] [[PubMed](#)]
51. Ostendorf, F.; Schmitz, C.; Hirth, S.; Kühnle, A.; Kolodziej, J.J.; Reichling, M. Evidence for Potassium Carbonate Crystallites on Air-Cleaved Mica Surfaces. *Langmuir* **2009**, *25*, 10764–10767. [[CrossRef](#)]
52. Trewby, W.; Livesey, D.; Voitchovsky, K. Buffering Agents Modify the Hydration Landscape at Charged Interfaces. *Soft Matter* **2016**, *12*, 2642–2651. [[CrossRef](#)]
53. Nečas, D.; Klapetek, P. Gwyddion: An Open-Source Software for SPM Data Analysis. *Cent. Eur. J. Phys.* **2012**, *10*, 181–188. [[CrossRef](#)]
54. Marek, J.; Demjénová, E.; Tomori, Z.; Janáček, J.; Zolotová, I.; Valle, F.; Favre, M.; Dietler, G. Interactive Measurement and Characterization of DNA Molecules by Analysis of AFM Images. *Cytom. Part A J. Int. Soc. Anal. Cytol.* **2005**, *63*, 87–93. [[CrossRef](#)] [[PubMed](#)]
55. Shao, Z.; Mou, J.; Czajkowsky, D.M.; Yang, J.; Yuan, J.Y. Biological Atomic Force Microscopy: What Is Achieved and What Is Needed. *Adv. Phys.* **1996**, *45*, 1–86. [[CrossRef](#)]
56. Gan, Y. Atomic and Subnanometer Resolution in Ambient Conditions by Atomic Force Microscopy. *Surf. Sci. Rep.* **2009**, *64*, 99–121. [[CrossRef](#)]